Original article

Institution of MECHANICAL ENGINEERS
Journal of MATERIALS: DESIGN AND APPLICATIONS

Proc IMechE Part L: J Materials: Design and Applications
1–13

DOI: 10.1177/14644207231173053
journals.sagepub.com/home/pil
Sage

Investigating energy absorption of thin-walled steel structures with combined mechanisms including inversion, folding and expansion

Ibrahem Waleed[1], Ali Abdul Kadhim Ruhaima[2], Zainab A Farhan[3], Nadia Salim Ismael[4], Muataz S Alhassan[5], Makram Skikara[6], Zeid Fadel Albahash[7,8] and Ahmed Najat Ahmed[9]

Abstract

In this research, thin-walled steel energy absorbers were investigated. The introduced structures absorb energy through the processes of inversion, folding and expansion. Each absorber consists of two end-capped frusta and a cylindrical shell. The intended absorbers were experimentally made and then tested. The mechanical properties of the used materials were extracted by performing tensile tests and then used for simulation. The simulations of this research were carried out using LS-DYNA software. After comparing the experimental and numerical results, a good agreement between the results was observed and then the obtained results were discussed. The intended absorbers were examined in terms of the thickness of the lower frustum, the height of the middle shell and the angle of the upper frustum. The obtained results showed that by increasing the thickness of the lower frustum, energy absorption in the inversion process increased. In addition, the investigations related to the effect of height on the collapse properties showed that increasing the height of the middle shell with a thickness of 2 mm for the lower frustum led to a decrease in energy absorption. Also, in the investigations carried out on the half angle of the frustum, it was found that the contribution of energy absorption in the expansion process was low.

Keywords

LS-DYNA, energy absorbers, thin-walled structures, expansion, folding, crashworthiness

Date received: 31 January 2023; accepted: 15 April 2023

Introduction

Thin-walled structures are used in many industries and different studies have been done on them.[1,2] Thin-walled energy absorbers are one of the types of structures that are used in the body of motor vehicles to reduce the weight and energy consumption[3,4] and also reduce the damage caused by traffic accidents as effectively as possible.[5] These structures can be made using sheets, produced by rolling,[6] shells and other types of raw materials. Energy absorbers reduce the injuries to the passengers during the accident. So far, different mechanisms have been introduced to absorb energy through energy absorbers, among which the mechanisms of inversion, folding, expansion and tearing can be mentioned. Each of these mechanisms prevents the transfer of destructive kinetic energy to the body of the devices in which the absorber is used by absorbing the energy caused by the force on the absorber. The materials used

[1]Medical Technical College, Al-Farahidi University, Baghdad, Iraq
[2]Al-Nisour University College, Baghdad, Iraq
[3]Air Conditioning and Refrigeration Techniques Engineering Department, Al-Mustaqbal University College, Babylon, Iraq
[4]Department of Construction Engineering & Project Management, AlNoor University College, Bartella, Iraq
[5]Division of Advanced Nano Material Technologies, Scientific Research Center, Al-Ayen University, Thi-Qar, Iraq
[6]Al-Esraa University College, Baghdad, Iraq
[7]College of Technical Engineering, Refrigeration and Air-Condition Technical Engineering Department, The Islamic University, Najaf, Iraq
[8]Ministry of Oil, Oil Exploration Company, Baghdad, Iraq
[9]Department of Computer Engineering, College of Engineering and Computer Science, Lebanese French University, Kurdistan Region, Iraq

Corresponding author:
Zainab A Farhan, Air Conditioning and Refrigeration Techniques Engineering Department, Al-Mustaqbal University College, Babylon, Iraq.
Email: zainab.abdul-kareem@uomus.edu.iq

in thin-walled structures include a wide range and can be classified into metal[7–9] and polymer materials. Regarding metal materials, ferrous metals aluminum and copper alloys can be mentioned. Energy absorbers have different processes to absorb energy and are tested under different loads.[10,11] Among them, we can mention the processes of inversion, folding, expansion and tearing.

As mentioned, one of the energy absorption processes is the inversion process, which has been studied comprehensively. Regarding the inversion of cylindrical shells, we can refer to the research.[12–14] Reddy et al.[13] experimentally and numerically introduced a new type of absorber using the inversion process. In their research, they used ABAQUS software for numerical simulations and proposed an optimal mode for their proposed absorber in terms of geometry. In reference,[14] absorbers using the inversion process were used in the manufacturing of car bumpers. In the reference,[15] Niknejad and Tavassolimanesh investigated the inversion process of capped-end frustum and extracted force–displacement curves for capped-end frusta analytically and experimentally.

The next process, which has taken up a major part of the research done on energy absorbers, is the folding process. The materials used for this type of absorber are mainly aluminum, steel, copper and brass. Alavi Nia and Chahardoli investigated and optimized aluminum nested structures in both experimental and numerical modes.[16,17] Steel structures were investigated in research.[18–20] Bardi and Kyriakides studied the mechanical properties of steel absorbers under axial compression[20] and observed the collapse modes including symmetric folding and diamond folding for cylindrical shells.

Numerous research has been carried out in relation to the expansion of cylindrical structures, which are mentioned in this section. In references,[21–26] the expansion of cylindrical shells by means of a rigid mandrel was investigated. In 2007, Shakeri et al.[25] studied the expansion of cylindrical thin-walled tubes as energy absorbers and calculated the amount of force required for the expansion of cylindrical shells in numerical, experimental and analytical situations under axial load. Yan et al.[26] experimentally and numerically investigated the expansion of thin-walled cylinders. In their research, they presented analytical relations for the necessary force required for expansion.

As previously mentioned, tearing is another mechanism of energy absorption processes in thin-walled structures and has been subject to numerous experimental, numerical and analytical researches. One of the most recent researches carried out on tearing is that of Shakib et al.[27] on the tearing of cylindrical shells. In this research, which was investigated experimentally and numerically, different cutters were considered and cylindrical shells were placed on them, and finally, the cylindrical shells were torn by applying axial compression in an extrusion process. In their research, LS-DYNA was used to simulate the tearing process. In addition to the studies, they did on the inversion of cylindrical shells, Reid also investigated the tearing process of steel structures experimentally.[12] Tearing of steel capped-end frusta was investigated in the research of Elahi et al.[28] In their research, they found the most optimal energy absorbers using the Taguchi method.

The absorbers that have been introduced so far are structures that absorb energy using a single mechanism. One of the problems facing energy absorber structures, especially structures that need a mandrel for collapse, is the final weight of the structures. In order to reduce the final weight of the structure in absorbers with the process of inversion, expansion and tearing, mandrels must be chosen as light as possible and in many cases hollow and even thin-walled. In addition, it is possible to introduce absorbers in which their thin-walled mandrels absorb energy through folding or other mechanisms. There have been some reports in this field, however, due to the scarcity of research there is room for more new mechanisms to be presented. In the research conducted by Zhang et al.,[29] structures with the simultaneous process of inversion and folding were introduced. The structures proposed by them were made of two frusta and cylindrical parts. Chahardoli et al.[30] proposed similar structures and used a thin-walled aluminum mandrel for collapsing to invert the aluminum capped-end

Figure 1. Materials used for conducting experimental tests.

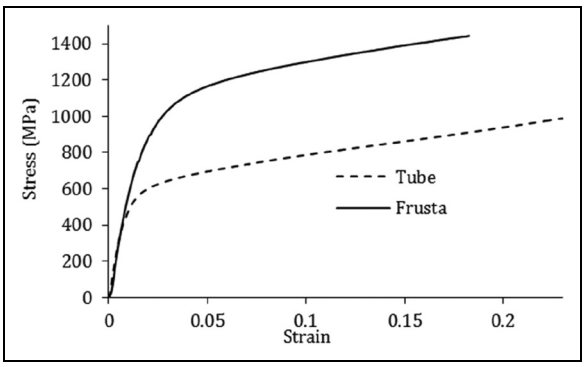

Figure 2. True strain–stress curves of steel for (a) capped-end frusta and (b) cylindrical shell.

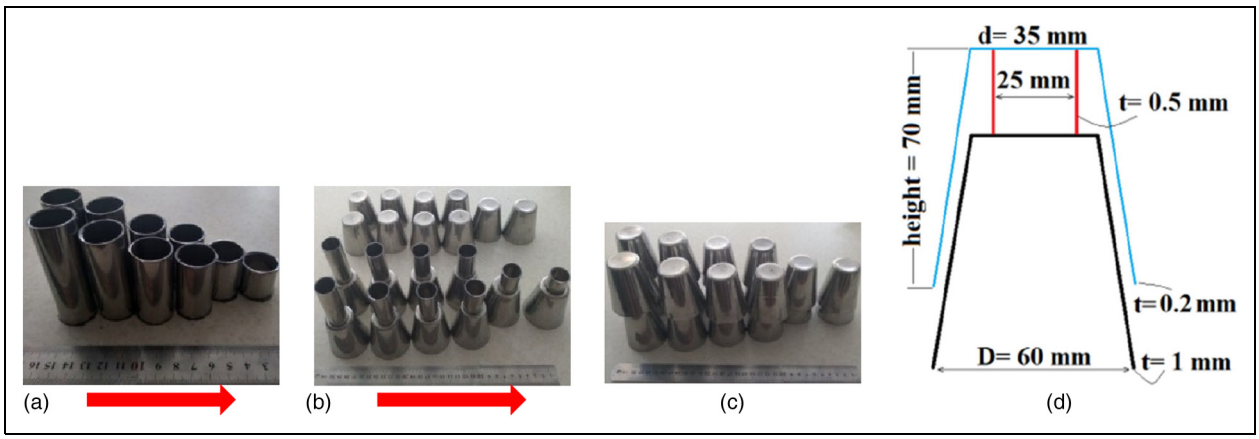

Figure 3. Samples prepared for quasi-static compression experimental tests, (a) cylindrical shell, (b) placement of cylindrical shells on the frusta, (c) final absorbers, (d) schematic view of the cross-section in the profile of the samples.

Table 1. Geometric characteristics of samples prepared for quasi-static compression tests (dimensions used are in mm).

Specimen	Lower frusta thickness	Upper frusta thickness	Upper and lower frusta height	Cylinder height	Cylinder diameter	Cylinder thickness
T75-10	1	0.2	70	75	25	0.5
T65-10	1	0.2	70	65	25	0.5
T55-10	1	0.2	70	55	25	0.5
T45-10	1	0.2	70	45	25	0.5
T35-10	1	0.2	70	35	25	0.5
T25-10	1	0.2	70	25	25	0.5

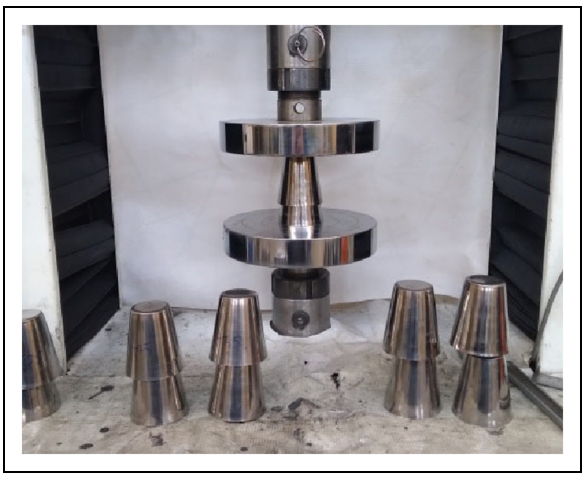

Figure 4. Placement of the samples in the machine to perform the quasi-static compression test.

frusta. In other studies conducted by Chahardoli et al., structures with simultaneous expansion-folding process were introduced.[31,32]

According to the stated introduction, thin-walled energy absorbers have always been considered by researchers, and efforts have been made to provide structures with the highest efficiency in terms of lightness and energy absorption. The structures proposed in this research were the types of structures that absorb energy using combined processes. The structures investigated in the past generally absorb energy through one mechanism. However, the absorbers introduced in this research can absorb energy by means of three processes of folding, expansion and inversion, which are the latest proposed absorbers. Considering that so far no research has been presented on the structures examined in this research, it was decided to study the effect of various factors on the collapse properties of these structures. The absorbers proposed in this research can be a suitable reference for the introduction and review of combined absorbers in the future.

Description of experimental tests

Tensile tests

The experimental tests of this research were carried out in two different groups. The first group was related to the experiments that were conducted on the raw materials in order to extract the mechanical properties. The second series was the experiments that were conducted to check the accuracy of the numerical simulations. In Figure 1, the materials used can be seen. As can be seen in this figure, steel tubes with a thickness of 0.5 mm and a diameter of 25 mm and capped-end frusta with two thicknesses of 0.19 and 1 mm were used. The diameter of the small and large base for the capped-end frusta was equal to 35 and 60, respectively, and their height was equal to

Table 2. Collapse characteristics of the simulated samples.

	Energy (kJ)	mass (g)	SEA (J/g)	Fm (kN)	d (mm)	Fa (kN)	CFE (%)
T25-10	5.17	119	43.5	236.5	82	63.1	26.7
T35-10	5.55	122	45.5	214.5	92	60.3	28.1
T45-10	6.16	125	49.3	172.5	100	61.6	35.7
T55-10	6.5	128	50.8	173.3	110	59.1	34.1
T65-10	5.41	131	41.3	163.1	113	47.9	29.4
T75-10	6.51	134	48.6	176.6	125	52.1	29.5
T25-15	8.25	166	49.7	261.1	83	99.4	38.1
T35-15	9.84	169	58.2	291.8	93	105.8	36.2
T45-15	10.61	172	61.7	285.7	103	103	36.1
T55-15	10.7	175	61.1	313.7	112.5	95.1	30.3
T65-15	11.32	178	63.6	299.6	122	92.8	31
T75-15	10.43	181	57.6	303.7	127.7	81.7	26.9
T25-20	13.15	213	61.7	369.2	84.5	155.6	42.1
T35-20	14.56	216	67.4	411.8	93	156.5	38
T45-20	15.64	219	71.4	473.4	102	153.3	32.4
T55-20	9.78	222	44.1	259	103.5	94.5	36.5
T65-20	11.15	225	49.5	271.6	117	95.3	35.1
T75-20	11.9	228	52.2	259.3	127.7	93.2	35.9

70 mm (the semi-angle of the used capped-end frusta was equal to 10.1°). To extract the mechanical properties of these materials, dumbbell-shaped samples were extracted from them and were subjected to tension in the machine at a speed of 4 mm/min, and the force curves in terms of displacement and then the stress curves in terms of true strain were extracted. Figure 2 shows the true stress–strain curves for the materials used.

Quasi-static compression tests

Figure 3 shows the samples prepared for quasi-static compression tests. As can be seen in this figure, these samples consist of several different parts that are placed on top of each other. Figure 3(a) shows the cylindrical shells prepared at heights of 25, 35, 45, 55, 65 and 75 mm. Figure 3(b) shows the placement of cylindrical shells on 1 mm thick frusta. And finally, it can be seen that in the final assembled samples as shown in Figure 3(c), the lower part is a 1 mm thick frustum on which a 0.5 mm thick cylindrical shell is placed and after that a frustum with a similar geometry and a thickness of 0.19 mm was placed on it. The geometric characteristics of these samples are given in Table 1. According to Table 1 and Figure 3, six different samples were tested, among which 4 samples (T75-10, T65-10, T55-10 and T45-10 samples) were tested with a repetition. In the naming of the samples in this table, the number after the letter T indicates the height of the cylindrical shell, and the second number is the thickness of the lower frustum in millimeters, which was multiplied by 10. In Figure 4, the sample placed on the device is shown.

Finite element model

Table 2 shows the simulated samples that were investigated in order to evaluate the effect of the thickness of the lower shell as well as the effects of the height of the cylindrical

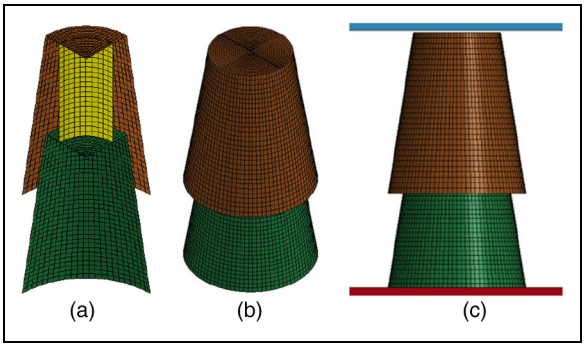

Figure 5. Example of finite element simulated in LS-DYNA software, (a) cross-section view, (b) perspective view, (c) front view.

shell. In this table, the absorbed energy is equal to the area under the force–displacement curve, and the specific energy is obtained by dividing absorbed energy by the mass of the structure. F_m shows the maximum force and F_a shows the average force in the force curve. Also, by dividing the average force by the maximum force, the crushing force efficiency or crush force efficiency (CFE) is obtained.

The simulation of the samples in this research was carried out using LS-DYNA finite element software. Using this software a static simulation was done with explicit method for energy absorbers. All the parts used for the absorber body were simulated as a Shell. Mat-piecewise-linear-plasticity was considered as the material model. CONTACT–AUTOMATIC–SURFACE–TO–SURFACE and CONTACT–AUTOMATIC–SINGLE–SURFACE algorithms were used to define the contact between rigid plates and shell elements and also between the shell elements themselves. Static and dynamic friction coefficients were 0.1 and 0.4. Figure 5 shows a sample of a cut finite element (Figure 5(a)) along with the full state in a three-dimensional view (Figure 5(b)). In these samples, the dimensions of the element used were 2 × 2 square millimeters for

Shell elements. The upper and lower plates (Figure 5(c)) were considered as Rigid parts, and the mechanical properties were selected according to the stress curves of Figure 1. Figure 6 shows the force–displacement curves for the samples where in the lower frusta thickness was 1 mm.

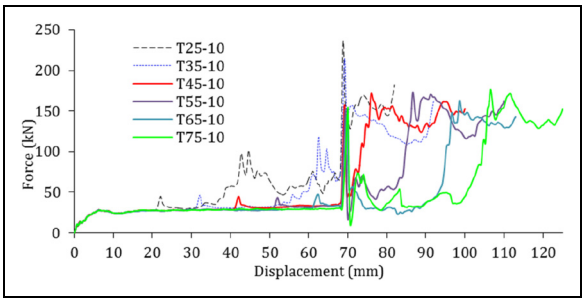

Figure 6. Force–displacement curves for samples whose thickness of the lower frusta is 1 mm.

Results and discussion

Validation of finite element results

The curves shown in Figure 6 were extracted experimentally. Figure 7 shows the difference between force–displacement curves for both experimental and numerical cases. Figure 8 shows the collapsed state of the tested samples next to the numerical samples. In Table 3, SEA and Fm parameters are compared. According to the agreement between the force–displacement curves and the collapsed states of the samples and also Table 3, we can confidently analyze the data with respect to the simulation results.

Investigating the effects of lower frusta thickness on the collapse properties

According to the results obtained in Table 2, the properties of collapse in different thicknesses for the lower

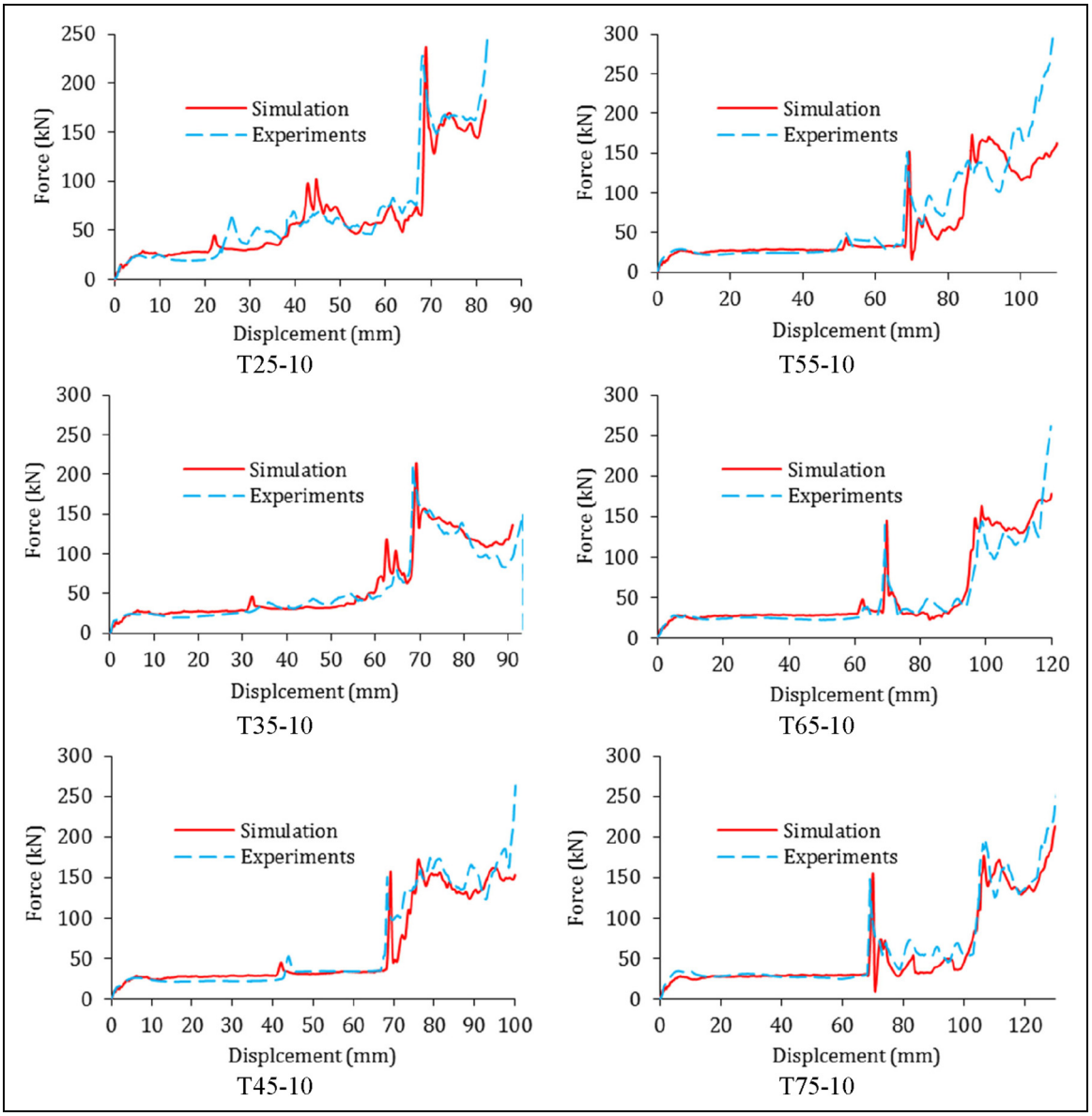

Figure 7. The difference between force–displacement curves for both experimental and numerical results.

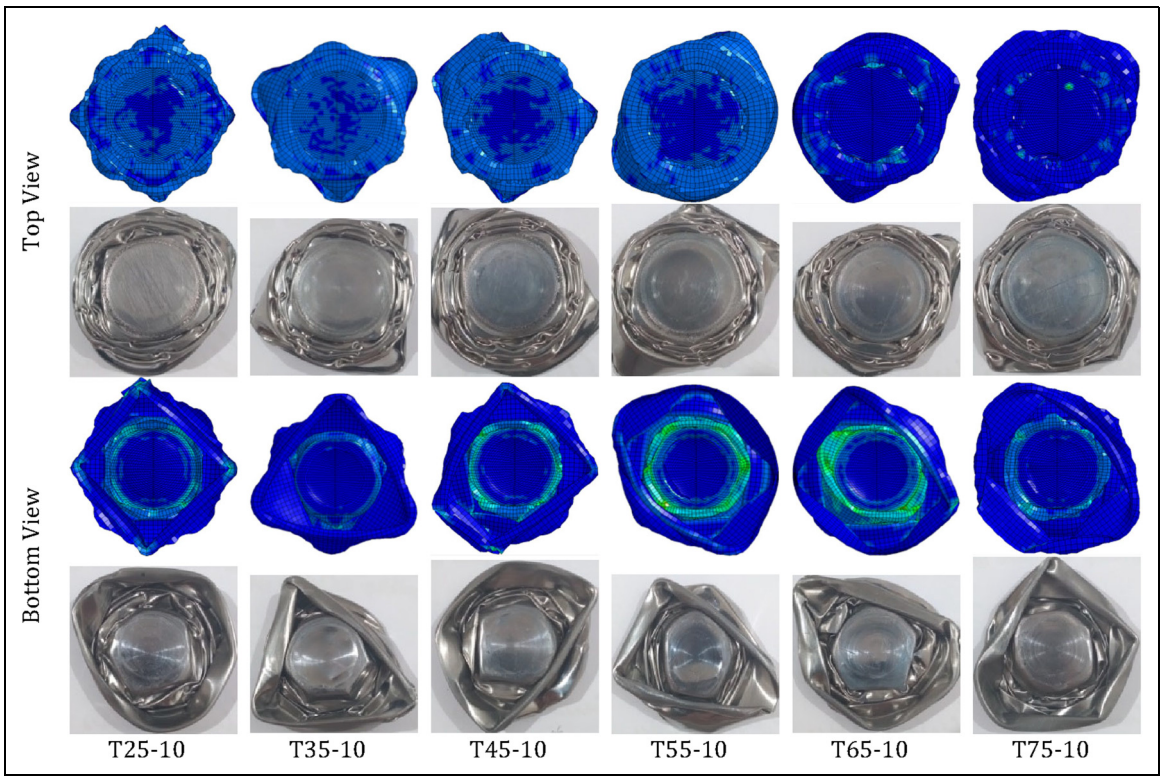

Figure 8. Comparison of collapsed state in experimental samples and corresponding simulated states.

Table 3. Difference between numerical and experimental results.

	SEA (J/g)			Fm (kN)		
Specimen code	Experimental	Numerical	Difference (%)	Experimental	Numerical	Difference (%)
T25-10	44.1	43.5	−1.4	232	236.5	1.9
T35-10	43.1	45.5	5.6	210	214.5	2.1
T45-10	52	49.3	−5.2	169.1	172.5	2
T55-10	53.1	50.8	−4.3	170.1	173.3	1.9
T65-10	40	41.3	3.2	159	163.1	2.6
T75-10	49.8	48.6	−2.4	171	176.6	3.3

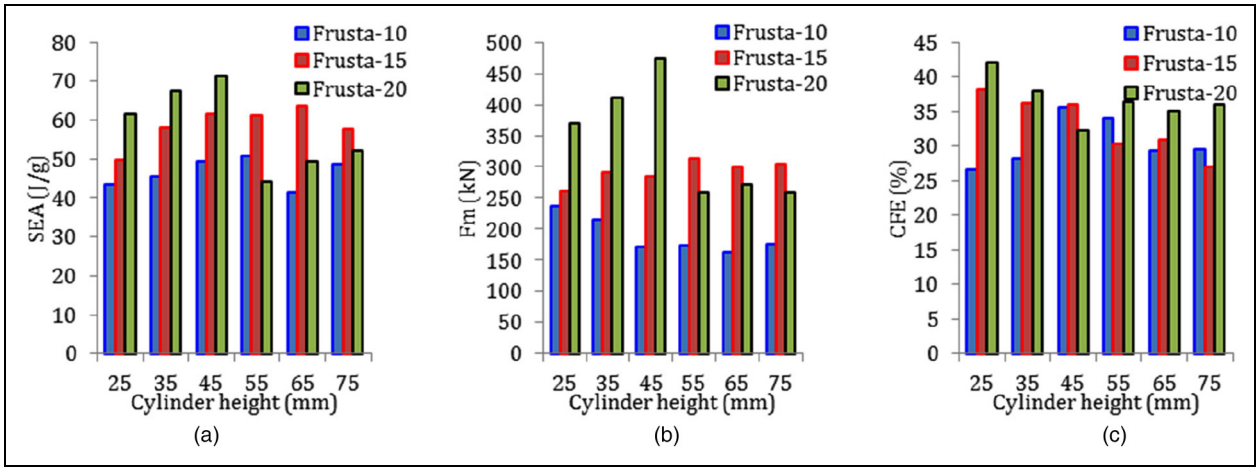

Figure 9. Investigating the effect of the thickness of the lower frusta on the collapse characteristics, (a) SEA parameter, (b) FM parameter, (c) crush force efficiency (CFE) parameter.

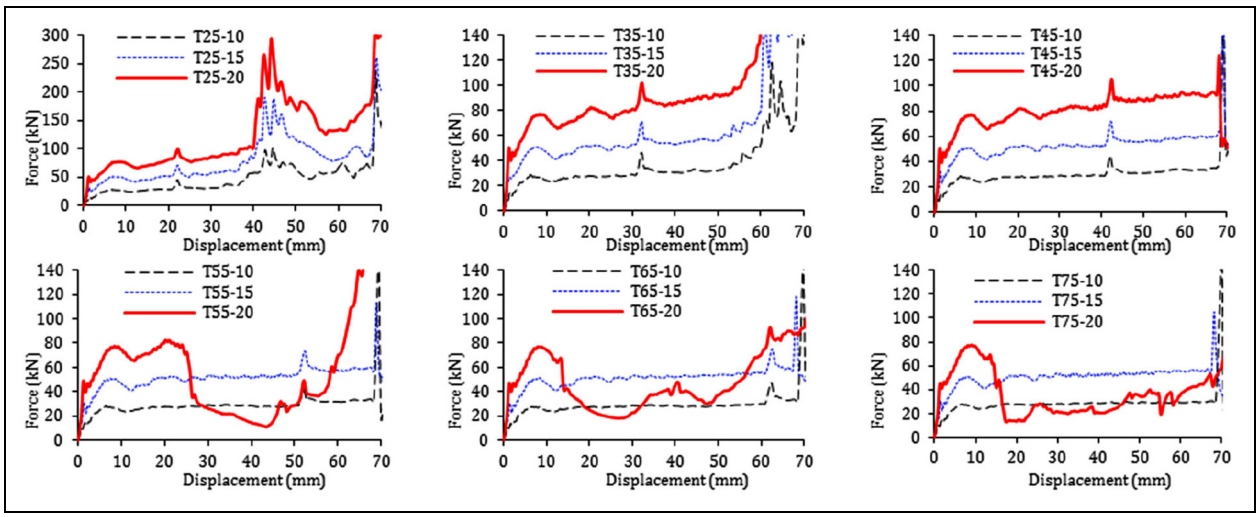

Figure 10. Effect of thickness on the inversion process.

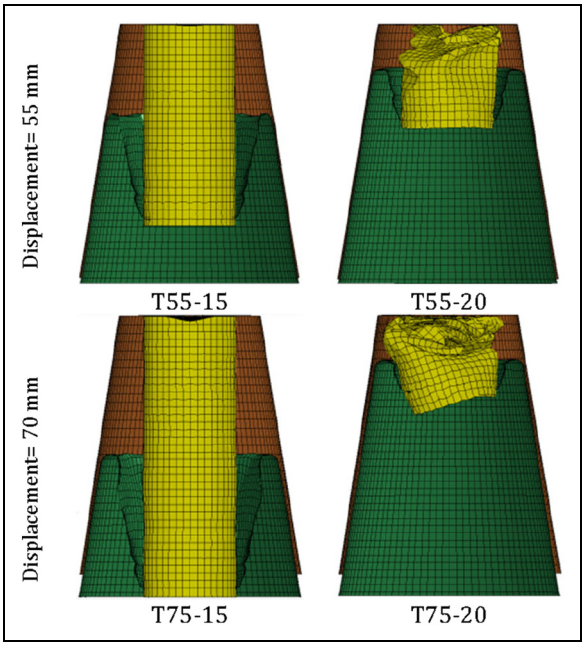

Figure 11. The effect of the thickness of the lower frusta on the inversion process (cut section).

frusta were investigated. The diagrams in Figure 9 show that in the samples proposed in this research, energy absorption and CFE can be increased by increasing the thickness of the lower frusta.

The main effect that increasing the thickness of the lower frusta has on the collapse process of the samples introduced in this research was related to the initial part of the collapse process. Figure 10 shows the force–displacement curves of the samples in the initial part of the collapse, which was related to the inversion process. According to Figure 10, when the height of the cylindrical shell is more than 45 mm, energy absorption of inversion was lower, compared to that of a cylindrical shell lower than 45 mm. In addition, when the height of the cylindrical shell is lower than 45 mm, the energy absorption increased with the increase in

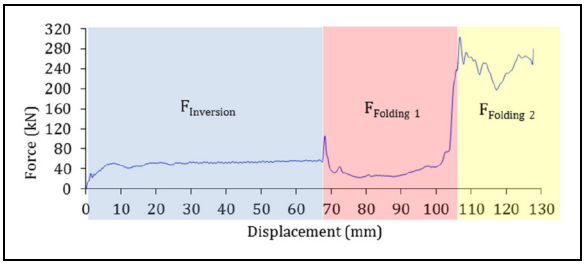

Figure 12. Division of force–displacement curve of sample T75-15 in terms of collapse process.

the height of the cylindrical shell. Folding of the cylindrical shell before complete inversion is the reason behind these differences. Also as can be seen in these figures, with the increase in thickness, energy absorption in the inversion process increased. However, different trends were observed for thicknesses 1, 1.5 and 2. According to Figure 10, in the thicknesses of 1 and 1.5, with the increase in the height of the cylindrical shell, the length of the lower frusta that undergoes inversion increased. In the case of samples with a thickness of 2 mm up to a height of 45 mm for a cylindrical shell, the inversion length increased, however, after this height, the inversion of the lower frusta decreased. The cessation of inversion in samples with shell height of 55, 65 and 75 was due to buckling or folding in the cylindrical shell, before the completion of the inversion process. In justifying this behaviour, it should be noted that with the advance of the shell into the frusta, the area of the frusta that should be inverted and a bending hinge created, increases and the thickness of 0.5 mm in the cylinder does not meet the necessary force to create inversion. In Figure 11, collapsed modes of samples T55-15, T55-20, T75-15 and T75-15 are compared in similar displacements. The shapes that show the collapsed state is in most cases cut and show the side view of the absorber.

To justify the increase in the force required for inversion due to the increase in the thickness of the shell, it is possible to use the previous research that was carried out in this field.

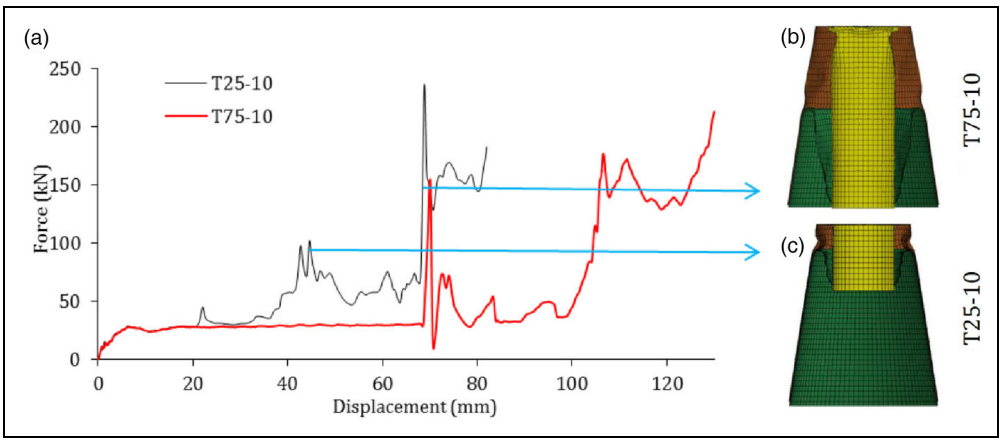

Figure 13. Comparison of the force curves of T75-10 and T25-10 samples along with cross-sections, (a) force–displacement curves, (b) collapse mode for T75-10, (c) collapse mode for T25-10.

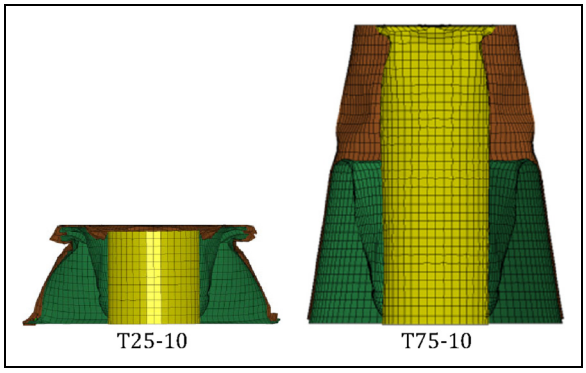

Figure 14. Comparison of the state of collapse of samples T25-10 and T75-10 in displacement of 70 mm.

According to the equation provided by Niknejad and Tavasolimanesh,[15] the necessary force in the inversion process of aluminum frustum was extracted according to equation (1). In this equation, d_0 is the diameter of the cylindrical shell, which is filled in accordance with reference,[15] and α represents the semi-angle of the capped-end frustum. R is the radius of curvature of the part of the frustum that is inverted and σ_0 indicates the yield stress. Finally, Δ is the penetration displacement or the displacement of the lower part of the cylindrical shell of this research. According to this equation, the force is a second-order function of the thickness of the frustum body and as it can be seen in this relationship, increasing the thickness leads to more force and energy absorption.

The force–displacement curve and consequently the energy–displacement curve of the samples introduced in this research can be divided into three different parts. The first part is related to the inversion process of the lower frustum, the force values of this process can be extracted according to equation (1). The second part is related to the simultaneous folding of the upper frustum and the cylinder shell. And finally, the third part is related to the continuation of the folding of the upper frustum and the cylindrical shell, to which the force necessary for the folding of the inverted frustum is added. The values of the average force required for the folding of a single cylindrical shell[33] and conical shell[34] can be extracted according to equations (2) and (3). In equation (2), D is the average diameter of the pipe, t is the thickness of the cylindrical shell and σ_0 is the yield stress of the cylindrical shell material. It must be said that equations (1) to (3) are to give qualitative guidance on the influence of parameters on each stage.

According to Figure 12, the amount of energy absorbed in each part can be written as equations (4) and (5). The absorbed energy in each force–displacement curve can be calculated according to equation (4). Considering that each curve in the graph of the introduced absorbers consists of three parts, the absorbed energy can be written in the form of equation (5) by considering the force of each part:

$$F_i = \frac{\pi\sigma_0 Rt}{2\Delta}[2-(\pi-2\alpha).\tan\alpha].[2\Delta+2R(\pi-2\alpha)\cos\alpha-(d-d_0)\cos\alpha]+\frac{\pi\sigma_0 Rt^2}{4R\Delta}\cdot\left[\frac{\Delta}{2\cos\alpha}+R\left(\frac{\pi}{2}-\alpha\right)-\frac{(d-d_0)}{4}\right]\cdot\left[\left\{\frac{\Delta}{2\cos\alpha}+R\left(\frac{\pi}{2}-\alpha\right)-\frac{(d-d_0)}{4}\right\}.\sin\alpha+d\right] \quad (1)$$

$$\bar{F}_f\,(\text{for Tube}) = 6\sigma_0 t\sqrt{Dt} \quad (2)$$

$$\bar{F}_f\,(\text{for Frusta}) = 3.4\sigma_0 t^{1.5} d^{0.5}\left(\frac{3\pi}{4}-\frac{\alpha}{2}\right)^{0.5} + 2.85\sigma_0 t^2\tan\alpha \quad (3)$$

$$E = \int F dx \quad (4)$$

$$E = E_{Inversion} + E_{Folding\,1} + E_{Folding\,2} \quad (5)$$

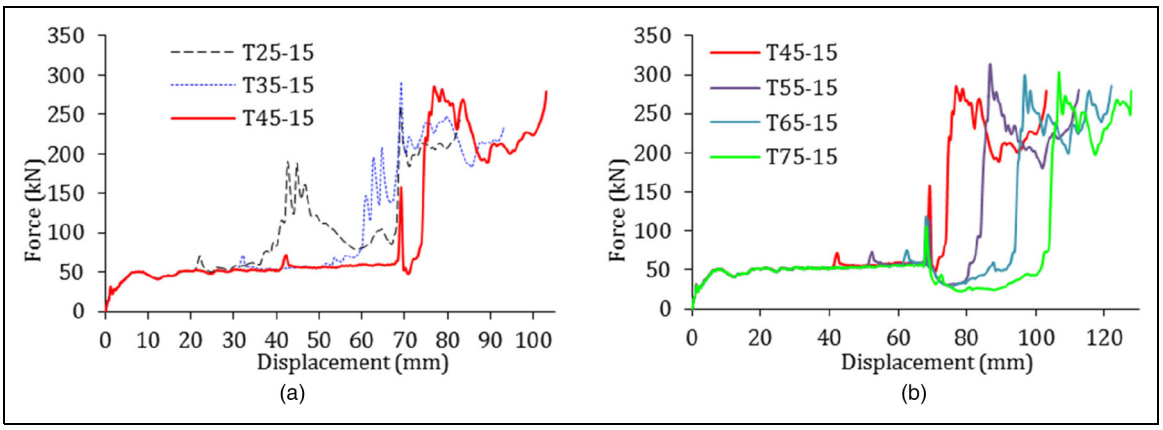

Figure 15. Comparison of force–displacement curves of samples with a thickness of 1.5 mm for the lower frusta, (a) lower heights and (b) high heights.

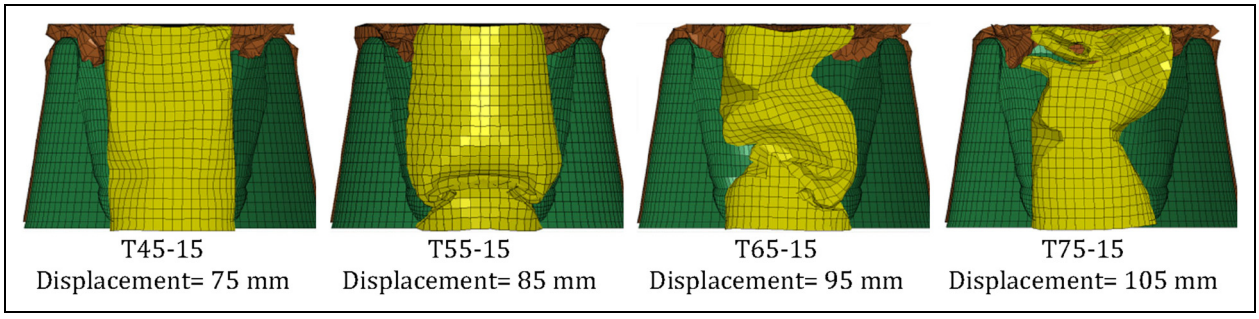

Figure 16. Cross section of samples T45-15, T55-15, T65-15 and T75-15.

Investigating the effect of cylindrical height in different samples

In the previous section, it was observed that the height of the cylindrical shell impacted the inversion process. In this part, more aspects of the effect of height on collapse properties are investigated. By comparing the force–displacement curves presented in Figure 13, which are related to the samples T25-10 and T75-10, it can be seen that in these samples, the height of the thin-walled cylinder also affects the collapse properties by affecting the maximum forces. As can be seen in Figure 13(a), for the T75-10 sample, the inversion process related to the lower frustum was fully completed compared to the T25-10 sample. The force peak appearing at 70 mm displacement of sample T75-10 was related to the beginning of folding in the cylindrical shell. The upper frustum is shown in Figure 13(b). It should be noted that in the displacement of 70 mm of sample T75-10, half of the frustum was inverted and the small base of the lower frustum reached its large base (Figure 13(b)), but in the case of sample T25-10, the displacement of the small base was approximately 25 mm (equal to the height of the cylindrical shell) and means that 12.5 mm of the lower frustum was inverted (Figure 13(c)). Figure 13(b) and (c) shows the location of the beginning of folding for both samples, in addition to corresponding to the peaks of force generated in approximate displacements of 25 mm and 75 mm for samples T25-10 and T75-10.

Regarding the higher maximum force of the T25-10 sample compared to the T75-10 sample at a displacement of 70 mm, we must refer to Figure 14. As can be seen in this figure, in the displacement of 70 mm of sample T75-10, the inversion process of the lower frustum is finished, and the force shown in the diagram is the sum of the force required to create folds in the upper frustum and the force required to fold the shell. But in the T25-10 sample, at a displacement of 70 mm, the force shown in the diagram is the sum of the forces required for: (1) the folding of the upper frustum, (2) the folding of the inverted part of the lower frustum, and (3) the folding of the cylindrical shell, which requires more power compared to the T75-10 sample.

In addition to the effect on the amount of maximum forces, the height of the middle shell also affects the location of their creation. Figure 15 shows the force curves of T45-15, T55-15, T65-15 and T75-15 samples. As can be seen in these examples, in addition to the maximum force appearing at the displacement of 70 mm, which is related to the beginning of folding of the upper frustum, maximum forces were created at the displacements of 75, 85, 95 and 105 mm. The maximum forces appearing in these displacements were due to the beginning of folding of the middle shell. The cut sections of samples T45-15, T55-15, T65-15 and T75-15 at displacements of 75, 85, 95 and 105 mm are shown in Figure 16.

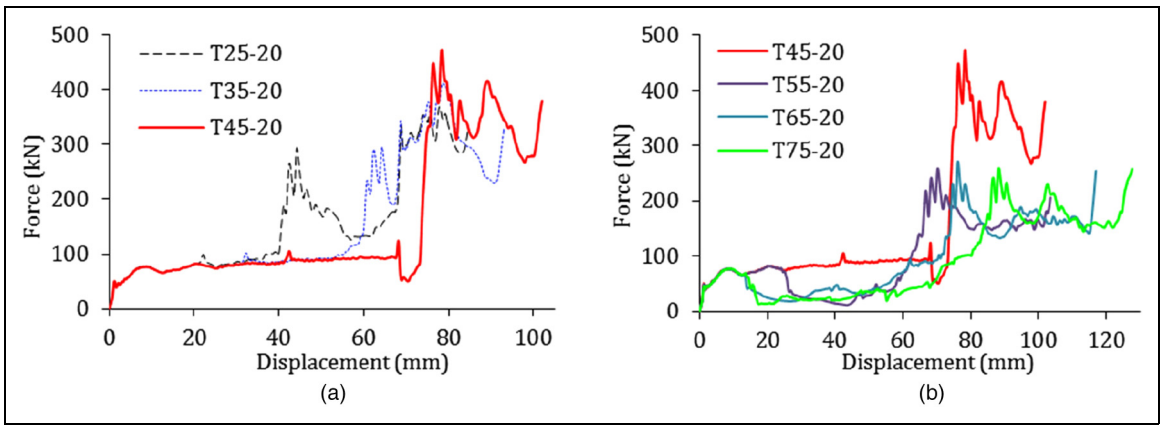

Figure 17. Comparison of the force–displacement curves of samples with a thickness of 2 mm for the lower frusta, (a) lower heights and (b) high heights.

By examining the graphs in Figure 17, it can be seen that in samples with a thickness of 2 mm for the lower frustum, increasing the height of the cylinder up to 45 mm leads to an increase in the maximum force and specific energy, and after that, increasing the height leads to a decrease in the specific energy and maximum force. The main reason for the reduction of the maximum force in the T55-20, T65-20 and T75-20 samples compared to the T45-20 sample is the general buckling in the cylindrical shell that occurs before the inversion process of the lower frustum is completed.

Investigating the effect of the upper frustum angle on the collapse process

What was done in this section of the research was to investigate the effect that the upper frustum semi-angle can have on the collapse properties. As mentioned before, to ensure uniformity in the force–displacement curve of the experimental samples, the lower frusta were selected from among frusta with a thickness of 1 mm and the upper frusta from among frusta with a thickness of 0.19 mm.

In this section, first, the combined collapse mechanism including inversion, folding and expansion has been explained using numerical results. Afterwards, the role of the upper frustum semi-angle with a thickness of 0.19 mm on the force curve and then the collapse properties were investigated. In order to create different angles, the small diameter of the upper frustum was fixed and equal to 35 mm and the large diameter values of 45, 50 and 60 mm were considered, which was equivalent to semi-angles of 4.1, 6.1 and 10.1. This is while the thickness and height of the lower frustum was equal to 1 and 70 mm and its semi-angle was equal to 10.1 mm. In other words, the small and large diameters were equal to 35 and 60, respectively; all three samples are shown in Figure 18. In these samples, the thickness, diameter and height of the cylindrical shell were 0.5, 25 and 65 mm, respectively.

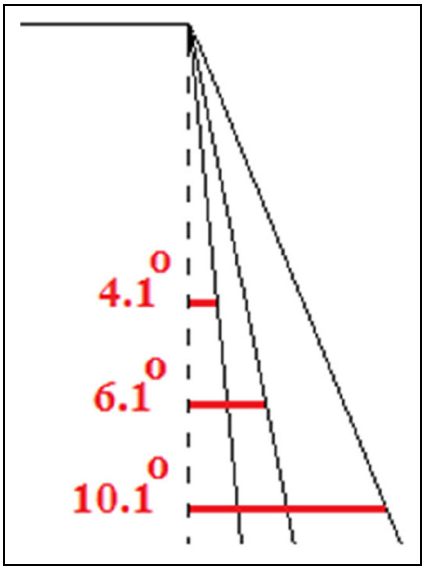

Figure 18. Semi-angles considered for the upper frustum with a thickness of 0.19 mm, a height of 70 and a small diameter of 35 mm.

The combined collapse mechanism including inversion, folding and expansion for T65-15-45 is shown in Figure 19. According to this figure, there are five different parts for force–displacement curve of T65-15-45. Collapse mode and also energy absorption of each part is shown in Figure 20.

Figure 21 shows the force curves for the tested samples. The numbers shown at the end of the name of the samples show the large diameter of the frustum. Figure 21(a) shows the force curve of the tested samples, and Figure 21(b) shows the force curve in the first 60 mm of collapse. In part b of Figure 21, the cylindrical shell inverts the lower frustum and simultaneously expands the upper frustum by moving downwards. Therefore, it can be said that in these samples, the processes of folding, expansion and inversion absorb energy. The cut section of sample T65-15-45 can be seen in Figure 22, in this figure it is clear that the lower

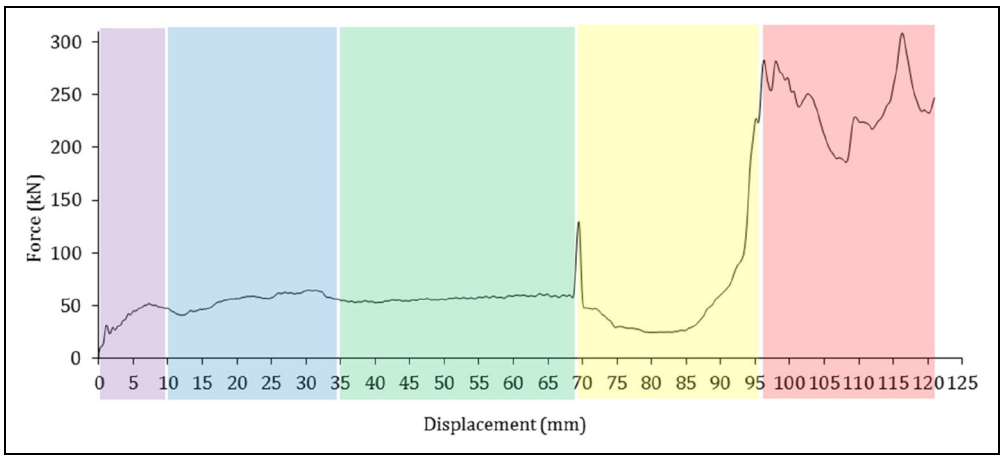

Figure 19. Force–displacement curve for T65-15-45 and its collapse procedure.

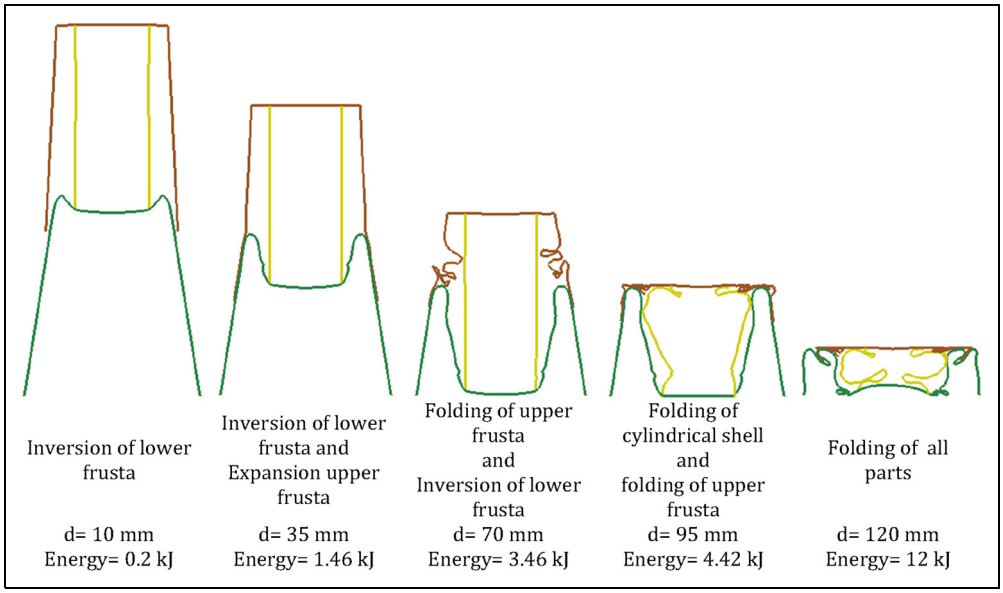

Figure 20. Collapse mode of T65-15-45 in different displacements and also its energy absorption.

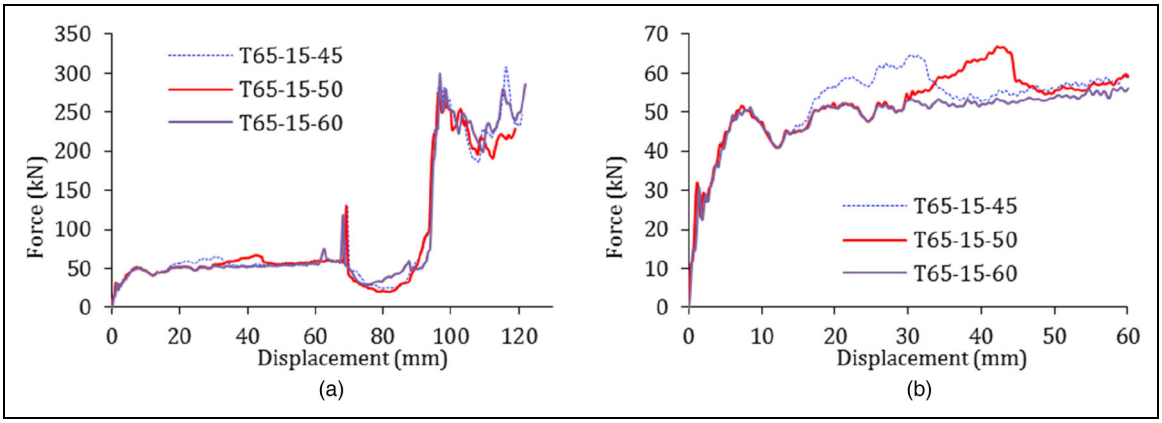

Figure 21. Force curves of samples with different frusta semi-angles (a) completely (b) in the initial 60 mm.

frustum was inverted and the upper frustum expanded. Further examination of the graphs in Figure 19(a), along with the fact that the surface under the graph shows the force–displacement diagram of the absorbed energy, indicates that the changes in the angle of the upper frustum did not have a high impact on the energy absorption capacity

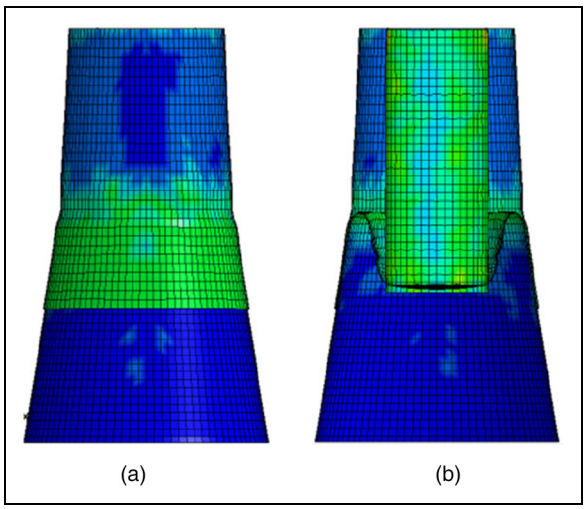

Figure 22. Simultaneous representation of the inversion of the lower frusta and the expansion of the upper frusta (a) complete sample, (b) cut section.

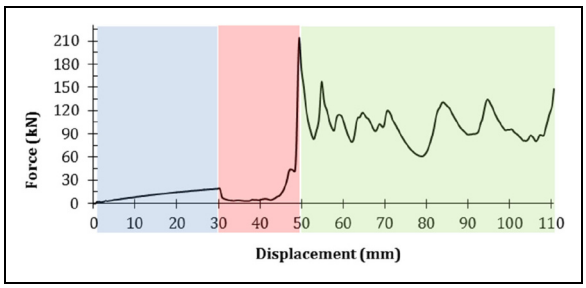

Figure 23. Force curve of sample T65-15-45 without middle cylindrical shell.

of the absorber. To further explain this issue, the T65-15-45 sample without the middle cylindrical shell was simulated and subjected to quasi-static loading. The force curve of this sample can be divided into three parts according to Figure 22. The first part was related to the expansion process of a part of the upper frustum. The second part of the folding process shows the part of the upper frustum that did not expand, and finally, the third part was the simultaneous folding process of the remaining parts. As can be seen in Figure 23, the area under the graph in the first part was lower than the other parts. In this case, to increase energy absorption, it is suggested that the upper frustum be made of softer materials such as aluminum to absorb more energy by increasing the expansion process and making the structure lighter. In addition to choosing another material for the upper frustum, an optimization problem can be defined in such a way that the upper frustum expands as much as possible without any folding in the lower frustum.

Conclusion

In this research, structures were presented that can simultaneously absorb energy through the processes of inversion, folding and expansion. The proposed structures were made of two steel capped-end frusta and a steel thin-walled cylindrical shell. The investigations carried out on the influence of the thickness of the frusta, the height of the cylindrical shell and the semi-angle of the expanding frusta led to the following results:

1. In the samples proposed in this research, energy absorption and crushing force efficiency could be increased by increasing the thickness of the lower frustum. It was also found that with the increase in the thickness of the lower frustum, energy absorption in the inversion process increased.
2. The results obtained in this research for absorbers with a 2 mm thickness of the lower frustum showed that increasing the height of the cylindrical shell did not lead to an increase in the inversion process. However, in samples with a thickness of 1 and 1.5 mm, the increase in the height of the cylindrical shell led to an increase in the length of the inversion process, followed by an increase in energy absorption through inversion.
3. The investigation of the absorbers with a lower frustum thickness of 2 mm showed that increasing the height of the cylinder up to 45 mm leads to an increase in the maximum force and specific energy, and after that the increase in height leads to a decrease in the absorbed energy and the maximum force.
4. Also, the investigations showed that the main reason for the reduction of the maximum force in the T55-20, T65-20 and T75-20 samples compared to the T45-20 sample was the general buckling in the cylindrical shell which took place before the completion of the inversion process of the lower frustum.
5. The investigations carried out in order to evaluate the effect of the proposed semi-angle of the upper frustum showed that the changes in the angle of the upper frustum did not have much effect on the energy absorption capacity of the introduced absorbers.

Declaration of conflicting interests

The author(s) declared no potential conflicts of interest with respect to the research, authorship, and/or publication of this article.

Funding

The author(s) received no financial support for the research, authorship, and/or publication of this article.

References

1. Dong Y, Shao P, Guo X, et al. Deformation characterization method of typical double-walled turbine blade structure during casting process. *J Iron Steel Res Int* 2023. DOI: 10.1007/s42243-022-00897-y.
2. Zhu Q, Chen J, Gou G, et al. Ameliorated longitudinal critically refracted – attenuation velocity method for welding residual stress measurement. *J Mater Process Technol* 2017; 246: 267–275.

3. Zhu Q, Chen J, Gou G, et al. Ameliorated longitudinal critically refracted—Attenuation velocity method for welding residual stress measurement. *J Mater Process Technol* 2017; 246: 267–275. DOI: 10.1016/j.jmatprotec.2017.03.022.
4. Chen L, Liu Q, Yang J, et al. Thermal expansion-quench of nickel metal-organic framework into nanosheets for efficient visible light CO2 reduction. *Chin Chem Lett* 2023; 34: 107335.
5. Zhang Y, Liu G, Ye J, et al. Crushing and parametric studies of polygonal substructures based hierarchical cellular honeycombs with non-uniform wall thickness. *Compos Struct* 2022; 299: 116087.
6. Zhu ZY, Liu YL, Gou GQ, et al. Effect of heat input on interfacial characterization of the butter joint of hot-rolling CP-Ti/Q235 bimetallic sheets by Laser + CMT. *Sci Rep* 2021; 11: 10020.
7. Tian L-m, Li M-h, Li L, et al. Novel joint for improving the collapse resistance of steel frame structures in column-loss scenarios, *Thin-Walled Struct* 2023; 182: 110219.
8. Jiang J, Ye M, Chen LY, et al. Study on static strength of Q690 built-up K-joints under axial loads. *Structures* 2023; 51: 760–775.
9. Yang Y, Lin B and Zhang W. Experimental and numerical investigation of an arch–beam joint for an arch bridge. *Arch Civil Mech Eng* 2023; 23: 101.
10. Zhang C and Abedini M. Application of Lagrangian approach to generate P-I diagrams for RC columns exposed to extreme dynamic loading. *Adv Concrete Const* 2022; 14: 153–167. doi: 10.12989/acc.2022.14.3.153
11. Abdullahi HS and Gao S. A novel multi-cell square tubal structure based on Voronoi tessellation for enhanced crashworthiness. *Thin-Walled Struct* 2020; 150: 106690.
12. Reid SR. Plastic deformation mechanisms in axially compressed metal tubes used as impact energy absorbers. *Int J Mech Sci* 1993; 35: 1035–1052.
13. Reddy TJ, Narayanamurthy V and Rao YVD. Evolution of a new geometric profile for an ideal tube inversion for crash energy absorption. *Int J Mech Sci* 2019; 155: 125–142.
14. Sohn SM, Kim BJ, Park KS, et al. Evaluation of the crash energy absorption of hydroformed bumper stays. *J Mater Process Technol* 2007; 187: 283–286.
15. Niknejad A and Tavassolimanesh A. Axial compression of the empty capped-end frusta during the inversion progress. *Mater Des* 2013; 49: 65–75.
16. Nia AA and Chahardoli S. Mechanical behavior of nested multi-tubular structures under quasi-static axial load. *Thin-Walled Struct* 2016; 106: 376–389.
17. Alavi Nia A and Chahardoli S. Optimizing the layout of nested three-tube structures in quasi-static axial collapse. *Thin-Walled Struct* 2016; 107: 169–181.
18. Zhu D-H, Zhong G-Q, Zeng J-J, et al. Behavior and model evaluation of large-rupture-strain (LRS) FRP-confined concrete-encased high-strength steel columns under axial compression. *Thin-Walled Struct* 2023; 183: 110367.
19. Ren W, Zhou X-H, Gao Y, et al. Compressive behavior of stiffened steel tubes for wind turbine towers. *Thin-Walled Struct* 2023; 183: 110372.
20. Bardi FC and Kyriakides S. Plastic buckling of circular tubes under axial compression – part I: experiments. *Int J Mech Sci* 2006; 48: 830–841.
21. Luo M, Yang J, Liu H, et al. Energy absorption of expansion tubes using a conical-cylindrical die: theoretical model. *Int J Mech Sci* 2019; 157–158: 207–220.
22. Moreno C, Winnett J and Williams T. On the effect of anisotropy on the performance and simulation of shrinking tubes used as energy absorbers for railway vehicles, *Thin-Walled Struct* 2021; 161: 107513.
23. Xie S, Cao Z, Yang G, et al. The energy absorption of a shrinking–expanding circular tube: an experimental and numerical investigation. *Thin-Walled Struct* 2023; 184: 110509.
24. Tan B, Yao S, Zhang L, et al. A novel deformation mode of expansion tubes accounting for extra contact. *Int J Mech Sci* 2023; 242: 108024.
25. Shakeri M, Salehghaffari S and Mirzaeifar R. Expansion of circular tubes by rigid tubes as impact energy absorbers: experimental and theoretical investigation. *Int J Crashworthiness* 2007; 12: 493–501.
26. Yan J, Yao S, Xu P, et al. Theoretical prediction and numerical studies of expanding circular tubes as energy absorbers. *Int J Mech Sci* 2016; 105: 206–214.
27. Shakib A, Magliaro J and Altenhof W. Maximum energy absorbing capacity and structural stability for energy dissipation devices exploiting a hybrid cutting/clamping deformation mode. *Thin-Walled Struct* 2023; 182: 110304.
28. Elahi SM, Rouzegar J and Assaee H. Axial splitting of conical frusta: experimental and numerical study and crashworthiness optimization. *Thin-Walled Struct* 2018; 127: 604–616.
29. Zhang X, Cheng G and Zhang H. Numerical investigations on a new type of energy-absorbing structure based on free inversion of tubes. *Int J Mech Sci* 2009; 51: 64–76.
30. Chahardoli S, Shabanzadeh M and Marashi SM. Introducing a new mechanism for energy absorption through simultaneous inversion-folding process. *Int J Crashworthiness* 2022; 27: 92–106. DOI: 10.1080/13588265.2020.1774481.
31. Chahardoli S and Nia AA. Investigation of mechanical behavior of energy absorbers in expansion and folding modes under axial quasi-static loading in both experimental and numerical methods. *Thin-Walled Struct* 2017; 120: 319–332.
32. Chahardoli S, Nia AA and Asadi M. Parametric investigation of the mechanical behavior of expanding-folding absorbers and their implementation in sandwich panels core, *Thin-Walled Struct* 2019; 137: 53–66.
33. Alexander JM. An approximate analysis of the collapse of thin cylindrical shells under axial loading. *Q J Mech Appl Math* 1960; 13: 10–15.
34. Mamalis AG, Manolakos DE, Saigal S, et al. Extensible plastic collapse of thin-wall frusta as energy absorbers. *Int J Mech Sci* 1986; 28: 219–229.